

EFFICIENT IMPACT ANALYSIS USING REDUCED FLEXIBLE MULTIBODY SYSTEMS AND CONTACT SUBMODELS

STEPHAN TSCHIGG and ROBERT SEIFRIED

Institute of Mechanics and Ocean Engineering
Hamburg University of Technology (TUHH)
Eißendorfer Straße 42, 21073 Hamburg, Germany
{stephan.tschigg, robert.seifried}@tuhh.de and www.tuhh.de/mum

Key words: Flexible Multibody Systems, Impacts, Contact Submodels

Abstract. For an efficient and accurate analysis of impact problems reduced flexible multibody systems can be used. Therefore, a precise reproduction of the wave propagation in the colliding bodies as well as contact forces and stresses are required. To capture all mentioned phenomena precisely, a set of eigenmodes and static shape functions has to be used for the elastic description of the flexible bodies. While the eigenmodes represent the global deformations, and therefore are physically important, the static shape functions are only necessary to capture the local deformations. Hence, their very high eigenfrequencies are artificially generated and additionally increase the numerical stiffness of the system. As a result of that, the numerical efficiency may decrease. In the present paper, two approaches for an efficient contact simulation in reduced flexible multibody simulations using static shape functions are presented. Both approaches are based on the subdivision of the elastic parts of the equations of motion in low and high frequency parts. The first approach uses modal damping on the high frequency parts. The second approach treats the high frequency parts quasi-statically and so they can be neglected in the dynamic simulation. The focus is on numerical stiff systems with a large number of static shape functions simultaneously loaded. Comparisons are made between reduced flexible multibody systems using the proposed approaches and full non-linear finite element simulations.

1 INTRODUCTION

One suitable approach for the efficient dynamical analysis of mechanical systems considering body flexibility is the method of flexible multibody systems (FMBS). In many dynamical systems, structural deformations can often be considered to be small and linear elastic. Hence, the floating frame of reference (FFoR) formulation is a suitable choice for the description of the body flexibility, see [1, 2]. In this method, the body-related frame undergoes large nonlinear motions and rotations. Furthermore, the small linear deformation of the body is described with respect to the reference frame.

Usually, the finite element (FE) method is used to model the body flexibility. In order to capture the local and global deformation effects in colliding bodies, a very fine discretized mesh is necessary. Due to the resulting large number of nodal degrees of freedom (DOF), the computation times are very high. For an efficient investigation of the system behavior, before and after impact, the approach of FMBS using reduced FE models combined with a contact model can be used. Hence, in the presented contribution, a combination of reduced FMBS and nodal contact calculation, see [3, 4], is presented.

In the case of collision between flexible bodies, the rigid body motion changes and local deformations occur. Furthermore, impacts may introduce high frequency wave phenomena. Hence, for the analysis of the dynamical behavior after impact, the contact forces, the stresses and the wave propagation are essential. Using a moderate number of eigenmodes to describe the reduced elastic body, the wave propagation is typically well approximated, see [4, 5, 6]. However, the local deformation and stresses in the contact area are poorly approximated using only a small number of eigenmodes. In addition, due to the missing local deformation there is no convergence behavior of the penalty factor observable when using the penalty contact formulation. Due to the missing local deformation, the contact stiffness is approximated too stiff. To compensate this stiff behavior, the penalty factor must be chosen relatively small. Therefore, increasing the penalty factor yields higher contact forces. Consequently, the simulation results depend strongly on the penalty factor, which has to be tuned heuristically to obtain good results, see [4, 6].

To capture the deformations in the contact area an additional set of static shape functions for each possibly loaded DOF can be used. However, these static shape functions introduce additional eigenfrequencies of very high magnitude to the reduced system, see [6, 7]. Due to these fast system components, the numerical stiffness increases. Consequently, the numerical efficiency decreases and non-physically high frequency oscillations may occur.

For an efficient and accurate impact simulation in reduced FMBS using static shape functions, two contact submodels, firstly presented in [6, 7], are used in this contribution. In both approaches, the elastic parts in the equations of motion of FMBS are divided in low and high frequency parts. According to [8], the low frequency parts represent the global motion in terms of wave propagation and the high frequency parts result from the local deformation. In a first approach, called damped contact submodel, proportional damping on the high frequency parts is used to reduce the influence of the high frequencies on the dynamic simulation. The second approach, called quasi-static contact submodel, initially presented in [6], is extended for a more efficient contact force evaluation in this contribution. In this second approach there is no need to determine suitable damping parameters. In order to investigate the limits of the contact submodels, numerical examples with a large number of nodal DOFs, resulting in many static shape functions simultaneously loaded and high numerical stiffness, are used.

The present work is organized in the following way. In Section 2 some basics of contact modeling in FMBS are briefly reviewed. This includes the model order reduction technique, the contact formulation and the mentioned contact submodels. In Section 3, numerical results of impacts of two bodies are presented. These results show the efficient

evaluation of the dynamic behavior, before and after impact, using the damped and the quasi-static contact submodel. Finally, in Section 4 a summary is given.

2 FLEXIBLE MULTIBODY MODEL

In this section, some fundamentals related to contact simulations with reduced FMBS are presented. At first the FFoR formulation is described. Then the model order reduction technique and the implemented contact formulation is presented. Subsequently, the used contact submodels are outlined.

2.1 Equations of motion

One frequent approach to take body flexibility into account in multibody systems is the FFoR formulation, see [1, 9]. In this approach, the motion of an elastic body is separated into a large non-linear rigid body motion of the moving reference frame and small deformations relative to this reference frame. In many applications of flexible multibody systems, the structural deformations are small and linear. In this case the elastic bodies can be efficiently described using the FFoR approach. The position vector of an arbitrary point P on the flexible body can be described by the sum of the large motion of the reference frame and small linear deformation. The deformation \mathbf{u}_P is approximated by the matrix of shape functions Φ and the time-dependent elastic coordinates \mathbf{q}_e as

$$\mathbf{u}_P(\mathbf{c}_{RP}, t) = \Phi(\mathbf{c}_{RP})\mathbf{q}_e(t). \quad (1)$$

In equation (1) the vector \mathbf{c}_{RP} represents the position of point P in the body-related frame. The vector of generalized coordinates of the system is given by $\mathbf{q} = [\mathbf{q}_r^T, \mathbf{q}_e^T]^T \in \mathbb{R}^f$, with the rigid coordinates $\mathbf{q}_r \in \mathbb{R}^{f_r}$ representing the rigid body degrees of freedom and the elastic coordinates $\mathbf{q}_e \in \mathbb{R}^{f_e}$ describing the elastic deformations, see [2]. Consequently, the equations of motion of a FMBS in minimal coordinates are given as

$$\underbrace{\begin{bmatrix} \mathbf{M}_{rr} & \mathbf{M}_{re} \\ \mathbf{M}_{er} & \mathbf{M}_{ee} \end{bmatrix}}_{\mathbf{M}} \underbrace{\begin{bmatrix} \ddot{\mathbf{q}}_r \\ \ddot{\mathbf{q}}_e \end{bmatrix}}_{\mathbf{h}} + \begin{bmatrix} \mathbf{0} \\ \mathbf{D}_{ee}\dot{\mathbf{q}}_e + \mathbf{K}_{ee}\mathbf{q}_e \end{bmatrix} = \underbrace{\begin{bmatrix} \mathbf{f}_{c,r} \\ \mathbf{f}_{c,e} \end{bmatrix}}_{\mathbf{f}_c} + \underbrace{\begin{bmatrix} \mathbf{h}_r \\ \mathbf{h}_e \end{bmatrix}}_{\mathbf{h}}. \quad (2)$$

The generalized mass matrix $\mathbf{M} \in \mathbb{R}^{f \times f}$ contains submatrices due to the rigid body motion \mathbf{M}_{rr} and the flexible body \mathbf{M}_{ee} , as well as the inertia coupling matrices \mathbf{M}_{er} and \mathbf{M}_{re} , see [1, 9] for further details. In equation (2) $\mathbf{K}_{ee} \in \mathbb{R}^{f_e \times f_e}$ and $\mathbf{D}_{ee} \in \mathbb{R}^{f_e \times f_e}$ are the stiffness and damping matrices of the generalized elastic coordinates and $\mathbf{f}_c \in \mathbb{R}^f$ is the vector of the generalized applied forces. In the vector $\mathbf{h} \in \mathbb{R}^f$ the generalized Coriolis, gyroscopic and centrifugal forces are summarized.

2.2 Model order reduction

A common way to describe the flexible body in equation (2) is the FE method. The linearized equations of motion of the FE model can be written as

$$\mathbf{M}_e\ddot{\mathbf{u}} + \mathbf{D}_e\dot{\mathbf{u}} + \mathbf{K}_e\mathbf{u} = \mathbf{f}_e, \quad (3)$$

with the vector $\mathbf{u} \in \mathbb{R}^{f_{\text{FE}}}$ containing the nodal displacements of the FE model. Here \mathbf{M}_e , \mathbf{D}_e , \mathbf{K}_e and \mathbf{f}_e are the mass matrix, damping matrix and stiffness matrix and the applied force vector of the FE model, respectively. Further, Rayleigh-damping is assumed. The direct integration of these FE models in the multibody simulation would result in a high dimension of the equations of motion. In order to reduce this number of DOFs, model order reduction methods are used.

The shape function matrix Φ shown in equation (1) is determined by linear model order reduction methods. In this work, the Craig-Bampton method, a special case of the Component Mode Synthesis is used for model order reduction, see [10]. In the Craig-Bampton method, the matrix $\Phi \in \mathbb{R}^{f_{\text{FE}} \times \hat{f}_e}$ is determined from selected eigenmodes as well as a set of constraint modes. These constraint modes are the static solution of the flexible body when a unit displacement is applied to each interface node. This matrix Φ fulfills the conditions of the Buckens-frame, see [1]. This yields the reduced mass matrix $\mathbf{M}_{ee} = \Phi^T \mathbf{M}_e \Phi$, damping matrix $\mathbf{D}_{ee} = \Phi^T \mathbf{D}_e \Phi$ and stiffness matrix $\mathbf{K}_{ee} = \Phi^T \mathbf{K}_e \Phi$ accordingly.

To consider dissipative effects, the reduced damping matrix \mathbf{D}_{ee} can be approximated by viscous damping, e.g. proportional damping. Using proportional damping, the eigenmodes of the undamped and the damped system agree, see [11, 12]. Based on this condition, the reduced system matrices can be transformed in diagonal form using mass-orthonormal eigenvectors as follows

$$\phi_i^T \mathbf{M}_{ee} \phi_j = \delta_{ij}, \quad \phi_i^T \mathbf{D}_{ee} \phi_j = 2\omega_i \xi_i \delta_{ij} \quad \text{and} \quad \phi_i^T \mathbf{K}_{ee} \phi_j = \omega_i^2 \delta_{ij}, \quad \text{with } i, j = 1 \dots \hat{f}_e. \quad (4)$$

Here, ξ_i denotes the modal damping parameter of the i -th eigenfrequency ω_i of the undamped reduced system. The Kronecker symbol δ_{ij} is equal to one for $i = j$ and equal to zero for every $i \neq j$.

2.3 Contact formulation

The contact model used in this contribution belongs to the penalty formulation and focuses on the frictionless normal contact. For an accurate contact force calculation, a precise three dimensional description of the contact area is necessary. Hence, a combination of nodal contact force calculation and reduced FMBS is used, see [3, 4]. Here, the surface elements from the underlying FE discretization are used as contact elements. For contact detection and force evaluation, this contact formulation uses node-to-surface elements as well as the contact situations node-to-edge and node-to-node. During time integration, in each time step the nodal coordinates of the contact area are determined using the generalized coordinates. Therefore, the efficiency of the contact algorithm is highly depending on the size of the contact area and the size of the matrix Φ . Subsequently, according to [1], the nodal contact forces are summarized in the generalized discrete forces \mathbf{f}_c .

2.4 Contact submodels

For an efficient contact simulation using reduced models considering static shape functions two approaches will be discussed in this section. In both approaches, the elastic

parts in equation (2) are subdivided according to [8] in low and high frequency parts. First, the elastic parts of the system are decoupled by solving the generalized eigenvalue problem and building mass-orthonormal eigenvectors, see [11]. Subsequently, the elastic coordinates in equation (2) can be divided in low frequency elastic coordinates $\mathbf{q}_e^{\text{lf}} \in \mathbb{R}^{J_e^{\text{lf}}}$ and high frequency elastic coordinates $\mathbf{q}_e^{\text{hf}} \in \mathbb{R}^{J_e^{\text{hf}}}$, such as

$$\begin{aligned} \begin{bmatrix} \mathbf{M}_{\text{rr}} & & \text{sym.} \\ \mathbf{M}_{\text{er}}^{\text{lf}} & \mathbf{M}_{\text{ee}}^{\text{lf}} & \\ \mathbf{M}_{\text{er}}^{\text{hf}} & \mathbf{0} & \mathbf{M}_{\text{ee}}^{\text{hf}} \end{bmatrix} \begin{bmatrix} \ddot{\mathbf{q}}_{\text{r}} \\ \ddot{\mathbf{q}}_{\text{e}}^{\text{lf}} \\ \ddot{\mathbf{q}}_{\text{e}}^{\text{hf}} \end{bmatrix} + \begin{bmatrix} \mathbf{0} & & \text{sym.} \\ \mathbf{0} & \mathbf{D}_{\text{ee}}^{\text{lf}} & \\ \mathbf{0} & \mathbf{0} & \mathbf{D}_{\text{ee}}^{\text{hf}} \end{bmatrix} \begin{bmatrix} \dot{\mathbf{q}}_{\text{r}} \\ \dot{\mathbf{q}}_{\text{e}}^{\text{lf}} \\ \dot{\mathbf{q}}_{\text{e}}^{\text{hf}} \end{bmatrix} \\ + \begin{bmatrix} \mathbf{0} & & \text{sym.} \\ \mathbf{0} & \mathbf{K}_{\text{ee}}^{\text{lf}} & \\ \mathbf{0} & \mathbf{0} & \mathbf{K}_{\text{ee}}^{\text{hf}} \end{bmatrix} \begin{bmatrix} \mathbf{q}_{\text{r}} \\ \mathbf{q}_{\text{e}}^{\text{lf}} \\ \mathbf{q}_{\text{e}}^{\text{hf}} \end{bmatrix} = \begin{bmatrix} \mathbf{f}_{\text{c,r}} \\ \mathbf{f}_{\text{c,e}}^{\text{lf}} \\ \mathbf{f}_{\text{c,e}}^{\text{hf}} \end{bmatrix} + \begin{bmatrix} \mathbf{h}_{\text{r}} \\ \mathbf{h}_{\text{e}}^{\text{lf}} \\ \mathbf{h}_{\text{e}}^{\text{hf}} \end{bmatrix}. \end{aligned} \quad (5)$$

The low frequency parts correspond to the global motion of the elastic body like the wave propagation. However, the high frequency parts are artificially generated by the static shape functions. They mostly represent the local deformations of the elastic body and have no effects on the low frequency global deformation. Hence, their dynamic contribution to the system dynamics can be neglected.

In this work, considering the eigenfrequencies of the decoupled elastic parts of the system, the separation frequency for distinction between low and high frequency parts is selected as follows. First of all, a sufficient number of eigenmodes to capture all global vibration effects in the frequency range of interest must be defined. Then, the eigenfrequency of the highest selected eigenmode represents the highest frequency of the low frequency parts. All frequencies of higher magnitude belong to the high frequency parts. Accordingly, all artificial frequencies introduced by the static shape functions belong to the high frequency terms. However, selecting the separation frequency as shown is only possible if the frequencies of the static shape functions are not in range of the low frequency parts.

In order to increase the numerical efficiency of the contact simulation a damped contact submodel was introduced in [6, 7]. In this first approach, modal damping is used to damp the eigenfrequencies inserted by the static shape functions. To capture the low frequency wave propagation, damping is used only on the high frequency parts. The main task is to identify the modal damping parameters ξ_i^{hf} using numerical studies. Firstly, the wave propagation should not be affected by the choice of ξ_i^{hf} . Secondly, the damping parameters should be large enough to increase the numerical efficiency sufficiently. In this work the damping parameters are calculated depending on the damped period $T_{\text{d},i}^{\text{hf}} = 2\pi/\omega_{\text{d},i}^{\text{hf}}$ with $\omega_{\text{d},i}^{\text{hf}} = \omega_i^{\text{hf}} \sqrt{1 - \xi_i^{\text{hf}}}$ and the undamped eigenfrequency ω_i^{hf} , as introduced in [6].

To avoid the determination of the unknown damping parameters using numerical studies, the quasi-static contact submodel, initially presented in [6], can be used in the contact simulation. After partitioning the decoupled equations of motion (5) it can be shown that the dynamical contribution of the high frequency parts to the system can be neglected. Using the Buckens-frame, a significant simplification of the equations of motion is possible, see [1]. But there is still an inconvenient coupling between rigid body motion and the

deformation of the elastic structure due to \mathbf{M}_{er} . In [8] it is shown, that the influence which inertia coupling of $\mathbf{M}_{\text{er}}^{\text{hf}}$ has on the equations of motion is smaller than the influence which inertia coupling of $\mathbf{M}_{\text{er}}^{\text{lf}}$ has. This is due to the specific characteristic of the high frequency parts, they only represent the local deformation. According to [8], the change of inertia is dominated by the low frequency parts, which represent the global deformation. Due to their specific characteristic, the local deformation has negligible influence on the mass moment compared to the global deformation and therefore the influence of high frequency parts $\mathbf{M}_{\text{er}}^{\text{hf}}$ is negligible. As a result of that, the vector $\mathbf{h}_{\text{e}}^{\text{hf}}$ is negligible too, see [8].

Neglecting $\mathbf{M}_{\text{er}}^{\text{hf}}$ is confirmed by [13] using numerical experiments. The high frequency elastic coordinates in equation (5) can be excited by the inertia coupling through $\mathbf{M}_{\text{er}}^{\text{hf}}$ as well as the generalized external forces $\mathbf{f}_{\text{c,e}}^{\text{hf}}$. In [13] it is shown, that the influence of the excitation by generalized external forces is significantly higher than the influence by inertia coupling effects and so the inertia coupling through $\mathbf{M}_{\text{er}}^{\text{hf}}$ can be neglected. Hence, neglecting damping, the last row of equation (5) can be simplified as

$$\mathbf{M}_{\text{ee}}^{\text{hf}} \ddot{\mathbf{q}}_{\text{e}}^{\text{hf}} + \mathbf{K}_{\text{ee}}^{\text{hf}} \mathbf{q}_{\text{e}}^{\text{hf}} = \mathbf{f}_{\text{c,e}}^{\text{hf}}. \quad (6)$$

This high frequency system represents the local deformation around the contact point. In low velocity impacts, the local deformation is quasi-static and therefore the inertia effects $\mathbf{M}_{\text{ee}}^{\text{hf}}$ can be neglected, see [8, 14]. However, the quasi-static influence of the displacement field

$$\mathbf{q}_{\text{e}}^{\text{hf}} = \mathbf{K}_{\text{ee}}^{\text{hf}^{-1}} \mathbf{f}_{\text{c,e}}^{\text{hf}}, \quad (7)$$

cannot be neglected. Especially, considering contact problems, the local displacement field and the global deformation is important for the accurate computation of the state-dependent contact forces $\mathbf{f}_{\text{c}}(\mathbf{q}_{\text{r}}, \mathbf{q}_{\text{e}}^{\text{lf}}, \mathbf{q}_{\text{e}}^{\text{hf}})$. The unknown elastic coordinates $\mathbf{q}_{\text{e}}^{\text{hf}}$ follow from the static equation (7) while the rigid coordinates \mathbf{q}_{r} and the low frequency elastic coordinates $\mathbf{q}_{\text{e}}^{\text{lf}}$ are available from the time integration. The evaluation of $\mathbf{q}_{\text{e}}^{\text{hf}}$ leads to the following system of nonlinear equations

$$\mathbf{f} = \mathbf{K}_{\text{ee}}^{\text{hf}^{-1}} \mathbf{f}_{\text{c,e}}^{\text{hf}}(\mathbf{q}_{\text{r}}, \mathbf{q}_{\text{e}}^{\text{lf}}, \mathbf{q}_{\text{e}}^{\text{hf}}) - \mathbf{q}_{\text{e}}^{\text{hf}} = \mathbf{0}, \quad (8)$$

which has to be solved iteratively by a Newton-Raphson method.

In [6] the schematic structure of the quasi-static contact submodel is presented. Solving equation (8), the Jacobian $\mathbf{J}(\mathbf{q}_{\text{e}}^{\text{hf}})$ is calculated in every iteration for a better approximation of $\mathbf{q}_{\text{e},n+1}^{\text{hf}} = \mathbf{q}_{\text{e},n}^{\text{hf}} + \Delta \mathbf{q}_{\text{e},n}^{\text{hf}}$ with $\Delta \mathbf{q}_{\text{e},n}^{\text{hf}} = -[\mathbf{J}(\mathbf{q}_{\text{e},n}^{\text{hf}})^{-1} \mathbf{f}_n]$ until the solution is found. In this work, the Jacobian $\mathbf{J}(\mathbf{q}_{\text{e}}^{\text{hf}})$ used in the Newton's method is computed only at the start of the contact force calculation or in case of slow convergence. During the iterations, the Jacobian is updated using Broyden's method, see [15], as

$$\mathbf{J}(\mathbf{q}_{\text{e},n+1}^{\text{hf}}) = \mathbf{J}(\mathbf{q}_{\text{e},n}^{\text{hf}}) + \frac{\Delta \mathbf{f}_{n+1} - \mathbf{J}(\mathbf{q}_{\text{e},n}^{\text{hf}}) \Delta \mathbf{q}_{\text{e},n+1}^{\text{hf}}}{\|\Delta \mathbf{q}_{\text{e},n+1}^{\text{hf}}\|^2} \Delta \mathbf{q}_{\text{e},n+1}^{\text{hfT}}, \quad (9)$$

with $\Delta \mathbf{q}_{\text{e},n+1}^{\text{hf}} = \mathbf{q}_{\text{e},n+1}^{\text{hf}} - \mathbf{q}_{\text{e},n}^{\text{hf}}$ and $\Delta \mathbf{f}_{n+1} = \mathbf{f}(\mathbf{q}_{\text{e},n+1}^{\text{hf}}) - \mathbf{f}(\mathbf{q}_{\text{e},n}^{\text{hf}})$. The Jacobian is updated using equation (9) until a maximum number of iterations is reached during root search.

Then, a new Jacobian will be computed. Compared to the quasi-static contact submodel presented initially in [6], the efficiency is significantly improved. Using this approach, the high frequencies of the static shape functions can be eliminated in the dynamic simulation. Thus, the numerical stiffness is reduced and larger time integration steps are possible. However, in each time step an additional system of nonlinear equations has to be solved.

3 NUMERICAL IMPACT STUDIES

To show the efficiency and the accuracy of the proposed contact submodels, first contact simulations using simple reduced FMBS are performed. The results focusing on the local and global deformation effects are validated with dynamic simulations using full dynamic FE simulations. For a correct evaluation of all deformation effects in the colliding bodies, a fine discretized mesh is necessary. Especially the contact region has to be discretized very finely to capture the deformations and stresses precisely. For all simulations the same computer, an Intel Xeon E3-1270v5 4x3.6 GHz with 64 GB RAM, is used.

The models used for numerical validation are composed according to [5] of a steel sphere (radius 15 mm) and two different aluminum rods, see Figure 1. At first, the impact of the sphere on a plane rod (radius 10 mm, length 1 m) is investigated. Then, to show the influence of large contact areas resulting in a large number of interface nodes, a rod with an inner radius of 20 mm is used. In both cases, the sphere's impact velocity is 0.3 m/s.

Using reduced bodies in the FMBS will inevitably lead to a stiff set of differential equations. Hence, the computation time increases and efficient formulas like the backward differentiation formulas have to be used for solving such stiff systems. In this contribution, the FMBS contact simulation is carried out using the MATLAB solver ode15s, see [16]. In stiff differential equations, using the ode15s, relatively large step sizes are possible.

3.1 Impact on planar rod

At first the impact of the steel sphere on the plane aluminum rod is investigated. The FE model of the rod consists of 342 984 nodal DOFs and the sphere consists of 64 086 nodal DOFs. Due to this large number of nodal DOFs, the computation time of the dynamic FE simulation is very high with about 697 mins in Abaqus. In the reduced model, for a precise approximation of the wave propagation in the rod, up to 200 eigenmodes are necessary. The static shape functions are calculated at 297 contact nodes (rod) and 261 contact nodes (sphere), resulting in 1085 and 802 elastic DOFs. To shorten computation times, only the DOFs in impact direction are considered when calculating the static shape functions. Numerical studies have shown that in case of the central impact the remaining DOFs can be neglected without losing accuracy. Thus, the reduced model of the rod consists of 491 elastic DOFs while the sphere consists of 280 elastic DOFs.



Figure 1: Model description - steel sphere and aluminum rod

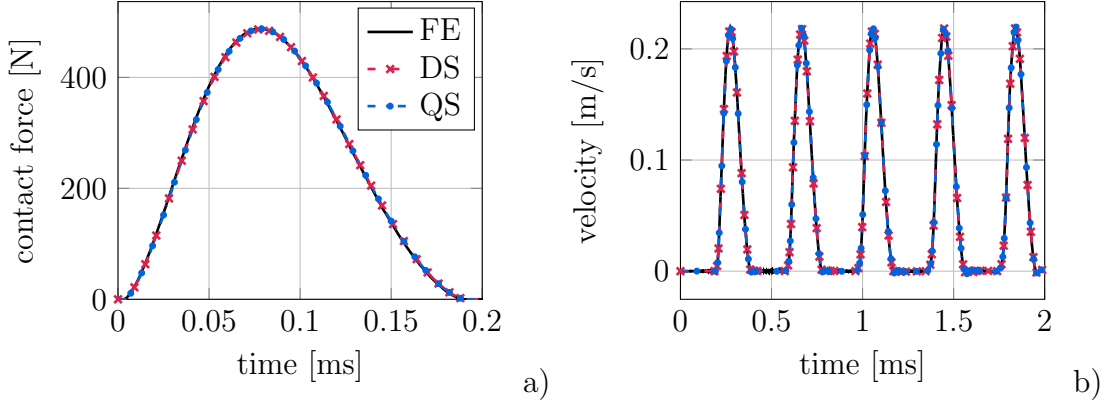


Figure 2: Contact forces a) and velocity at the rod end b) (plane rod) (FE: finite element results, DS: damped contact submodel, QS: quasi-static contact submodel)

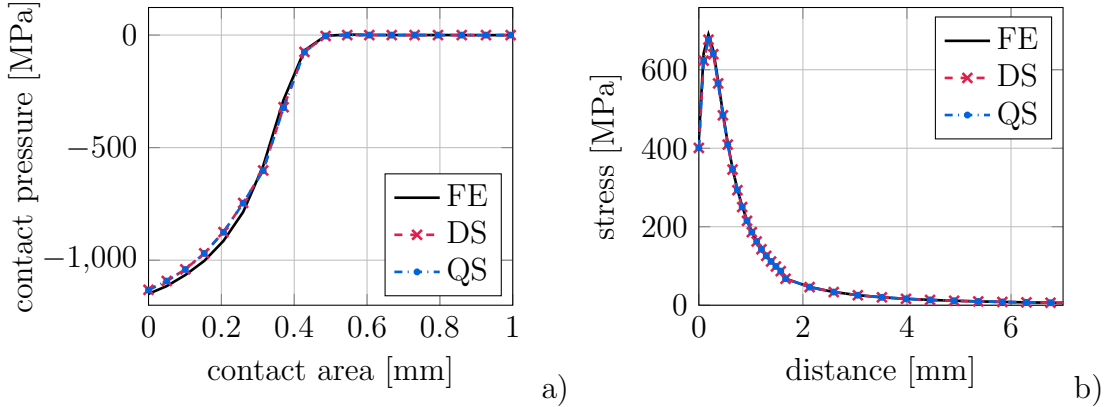


Figure 3: Contact pressure in contact area a) and stresses on symmetry axis of rod b) (plane rod) (FE: finite element result, DS: damped contact submodel, QS: quasi-static contact submodel)

The eigenfrequencies of the inner modes are up to 69 kHz (rod) and 131 kHz (sphere). However, the eigenfrequencies introduced by the static shape functions are up to 21 MHz (rod) and 18 MHz (sphere). During impact, the contact forces excite all vibration modes and very small step sizes are necessary during time integration to capture the fast components. Consequently, the numerical stiffness increases significantly. Due to the high numerical stiffness, the step sizes have to be very small and the convergence of the simplified Newton iteration in the ode15s, see [16], is very slow. Without material or numerical damping or using the quasi-static contact submodel, the computation times of the FMBS would be significantly higher than the computation times of the FE simulation. For this reason, impact simulations using undamped models are not reasonable.

In order to increase the computational efficiency, the damped contact submodel is used first. For this purpose, the modal damping parameters have to be identified. As presented in Section 2.4, the damping parameters of the high frequency modes are calculated using

the damped period $T_{d,i}^{\text{hf}}$. Therefore, the damped periods for all high frequency modes are adjusted to an equal value. For an efficient simulation, the damped period $T_{d,i}^{\text{hf}}$ has to be selected as large as possible for large step sizes, but small enough that there is no influence on the wave propagation. Furthermore, the choice of the damping parameters in the transition area between low and high frequency parts has great influence on the numerical efficiency, see [6].

Numerical studies have shown that a damped period of $T_{d,i}^{\text{hf}} = 5e^{-7}\text{s}$ and damping parameters of $\xi_i^{\text{hf}} = 0.05$ in the transition area are a good choice in terms of efficiency and accuracy for the system rod–sphere. The contact force of the FMBS simulation is in very good agreement with the FE results, see Figure 2a). As shown in Figure 2b), the global motion of the rod can be approximated very well, too. Damping only the high frequency parts, there is no negative influence on the wave propagation. The contact pressure and the stresses on the symmetry axis of the rod shown in Figure 3 agree very well with the FE results. The stresses in the FMBS are recovered using stress modes, see [17]. Consequently, the local deformation is approximated very well, too. Due to the good approximation of the local deformation, a convergence behavior of the penalty factor is observable. Using the damped contact submodel, a reasonable investigation of this numerically stiff system is possible at all. But the computation time with about 280 mins is still relatively high.

In order to further improve the efficiency, the quasi-static contact submodel, presented in Section 2.4, is used. The results of the sphere impacting the plane rod are shown in Figure 2 and Figure 3. Again a very good agreement of contact force, wave propagation and stresses in the contact area are observed. The computation time can be reduced significantly to about 23 mins. Furthermore, the results considering all global and local deformation effects are in very good agreement with the FE results. In addition, it is observed, that the simulation results do not change when further increasing the penalty factor.

3.2 Impact on rod with inner radius

The next investigation focuses on larger contact areas with a higher number of static shape functions simultaneously loaded. For this purpose, the rod is modeled with an inner radius of 20 mm. The geometry of the sphere remains unchanged as well as the impact velocity of 0.3 m/s. The contact radius of the plane rod, shown in Section 3.1, is about 0.5 mm. Using the rod with inner radius, the contact radius increases up to 1 mm. Therefore, the number of static shape functions in the contact area increases, too. Compared to the previously presented FE model, the discretization in the contact area is now slightly coarser. Hence, the rod consists of 281 196 nodal DOFs and the sphere consists of 58 536 nodal DOFs. Then, the computation time of the dynamic FE simulation is about 434 min. Again 200 eigenmodes are used in the reduced description to capture the wave propagation in the rod. For the calculation of the static shape functions 393 contact nodes (rod) and 385 contact nodes (sphere) are used which leads to 1373 (rod) and 1174 (sphere) elastic DOFs. Considering the DOFs in impact direction, 587 (rod)

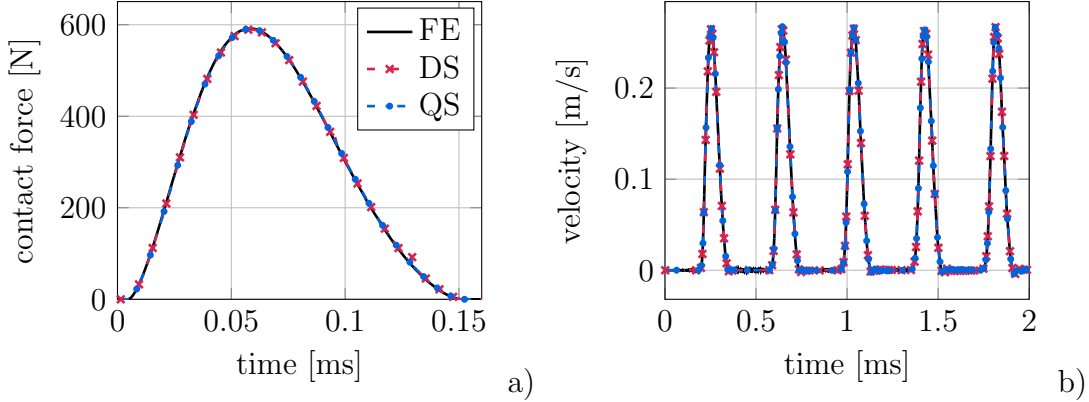


Figure 4: Contact forces a) and velocity at the rod end b) (rod inner radius) (FE: finite element results, DS: damped contact submodel, QS: quasi-static contact submodel)

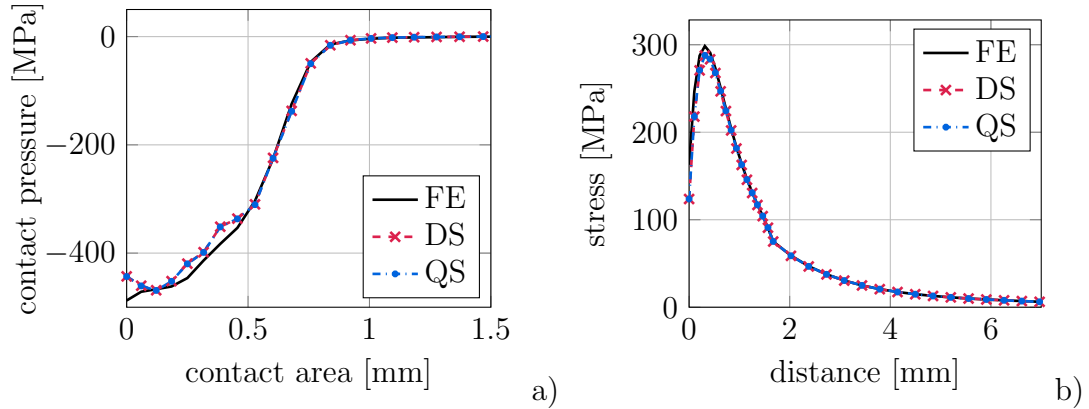


Figure 5: Contact pressure in contact area a) and stresses on symmetry axis of rod b) (rod inner radius) (FE: finite element results, DS: damped contact submodel, QS: quasi-static contact submodel)

and 404 (sphere) elastic DOFs remain. While the eigenfrequencies of the inner modes remain the same, the eigenfrequencies introduced by the static shape functions are up to 22 MHz (rod) and 30 MHz (sphere).

Numerical studies have shown, that a damped period $T_{d,i}^{\text{hf}} = 5e^{-7}\text{s}$ and the damping parameter $\xi_i = 0.05$ in the transition area are suitable values for the investigated system. The results of the damped FMBS simulation are shown in Figure 4 and 5. The contact force and the wave propagation in the rod are in very good agreement with the FE results. Compared to the plane rod, the contact duration is shorter and the contact force is higher using the rod with inner radius, see Figure 2a) and 4a). Furthermore, the impact on the rod with inner radius yields stronger wave excitations compared to the plane rod, see Figure 2b) and 4b). The stress analysis, presented in Figure 5, shows that the impact on the rod with inner radius creates smaller stresses since the contact force is distributed on a larger area. Due to the large number of elastic DOFs and the

high numerical stiffness caused by high eigenfrequencies, the computation time using the damped contact submodel is about 513 min and underperforms the FE model.

Again, in order to further increase the efficiency, the quasi-static contact submodel is used. The results shown in Figure 4 and 5, are in very good agreement with the FE results and the results of the damped contact submodel. Compared to the damped contact submodel and FE simulation, there is a major reduction of computation time to about 46 min. The FMBS contact simulations show slightly larger deviations in the contact pressure and stresses compared to the FE model, see Figure 5. This may result from the coarser discretization in the contact area. Nevertheless, due to the precise modeling of the local deformation a convergence behavior of the penalty factor is observable in both submodels.

4 CONCLUSIONS

In impact simulations using reduced FMBS, besides global vibration modes, a large number of static shape functions are often necessary for the detailed analysis of the local and global deformation effects. Extending the reduction basis by static shape functions, additional eigenfrequencies of high magnitude are added to the reduced system. Hence, the numerical stiffness increases. For an efficient investigation of those models, in the present work, different approaches have been presented. In both approaches the equations of motion are divided in low and high frequency parts. The first approach uses modal damping on the high frequency parts, to increase the numerical efficiency. Using the damped contact submodel, the results are in very good agreement with the FE reference results, but the computation times are still very high. Especially in simulations like the rod with inner radius considering a large number of static functions, the limit of the damped contact submodel is reached. It is not possible to find appropriate damping parameters to reduce the numerical stiffness on the one hand and not affect the wave propagation on the other hand. Thus, the damped contact submodel is limited to less stiff systems or less elastic DOFs. In the quasi-static contact submodel approach, the inertia coupling between rigid body motion and the deformation of the high frequency parts is neglected. By treating the high frequency parts quasi-statically, they can be removed from the equations of motion. With this approach, the numerical efficiency is significantly enhanced compared to the damped contact submodel. Nevertheless, the results are in very good agreement with the FE reference simulation. The presented simple numerical examples illustrates the advantage of the quasi-static contact submodel in impact simulations considering a large number of static shape functions and high numerical stiffness.

REFERENCES

- [1] Schwertassek, R. and Wallrapp, O. *Dynamik flexibler Mehrkörpersysteme: Methoden der Mechanik zum rechnergestützten Entwurf und zur Analyse mechatronischer Systeme*. Vieweg, 1999.
- [2] Seifried, R. *Dynamics of Underactuated Multibody Systems - Modeling, Control and Optimal Design*. Springer, 2014.

- [3] Ziegler, P. *Dynamische Simulation von Zahnradkontakten mit elastischen Modellen (in German)*. Dissertation, Schriften aus dem Institut für Technische und Numerische Mechanik der Universität Stuttgart. Shaker Verlag, Vol. 23, 2012.
- [4] Tamarozzi, T., Ziegler, P., Eberhard, P. and Desmet, W. Static modes switching in gear contact simulation. *Mech. Machine Theory* (2013) **63**:89-106.
- [5] Schiehlen, W. and Seifried, R. Three approaches for elastodynamic contact in multi-body systems. *Multibody Syst. Dyn.* (2004) **12**:1-16.
- [6] Tschigg, S. and Seifried, R. Efficient evaluation of local and global deformations in impact simulations in reduced flexible multibody systems based on a quasi-static contact submodel. *Proceedings of the ECCOMAS Thematic Conference on Multibody Dynamics* (2017) **8**:315-325.
- [7] Tschigg, S. and Seifried, R. Impact simulations using a quasi-static contact submodel in reduced flexible multibody systems. *PAMM* (2016) **16**:63-64.
- [8] Sherif, K., Witteveen, W. and Mayrhofer, K. Quasi-static consideration of high-frequency modes for more efficient flexible multibody simulations. *Acta Mechanica* (2012) **223**:1285-1305.
- [9] Shabana, A. A. *Dynamics of Multibody Systems*. Cambridge Univ. Press, 3rd Edition, 2005.
- [10] Craig, R. and Bampton, M. Coupling of substructures for dynamic analyses. *AIAA J.* (1968) **6**:1313-1319.
- [11] Lehner, M. *Modellreduktion in elastischen Mehrkörpersystemen (in German)*. Dissertation, Schriften aus dem Institut für Technische und Numerische Mechanik der Universität Stuttgart. Shaker Verlag, Vol. 10, 2007.
- [12] Adhikari, S. Damping modelling using generalized proportional damping. *J. Sound Vibr.* (2006) **293**:156-170.
- [13] Heirman, G. H. K., Tamarozzi, T. and Desmet, W. Static modes switching for more efficient flexible multibody simulation. *Int. J. Num. Meth. Eng.* (2011) **87**:1025-1045.
- [14] Seifried, R., Schiehlen, W. and Eberhard, P. The Role of the Coefficient of Restitution on Impact Problems in Multibody Dynamics. *J. Multi-body Dyn.* (2010) **224**:279–306.
- [15] Hermann, M. *Numerische Mathematik*. Oldenbourg Verlag, 2011.
- [16] Shampine, L. F. and Reichelt, M. W. The MATLAB ODE Suite. *SIAM J. Sci. Comput.* (1997) **18**:1-22.
- [17] Tobias, C. and Eberhard, P. Stress recovery with Krylov-subspaces in reduced elastic multibody systems. *Multibody Syst. Dyn.* (2011) **25**:377-393.